The influence of particle composition on Thorium scavenging in the Mediterranean Sea

M. Roy-Barman, C. Lemaitre, S. Ayrault, C. Jeandel, M. Souhaut, J.C. Miquel

The influence of particle composition on Thorium scavenging in the Mediterranean Sea

M. Roy-Barman (1)*, C. Lemaître (1,2), S. Ayrault (1), C. Jeandel (3), M. Souhaut (3), J.-C. Miquel (4)

(1) LSCE/IPSL Laboratoire CNRS/CEA/UVSQ, 91198 Gif-sur-Yvette Cedex, France

(2) LATMOS (IPSL/ UVSQ / CNRS / Paris VI), 75252 Paris Cedex 05, France

(3) LEGOS (CNRS/CNES/IRD/UPS), Observatoire Midi-Pyrénées, 14, Av. E. Belin, 31400 Toulouse, France.

(4) IAEA Marine Environment Laboratories, 4 Quai Antoine 1er, MC-98000, Monaco

Final version

* corresponding author : Phone: (33)1-69-82-35-66; Fax: (33)1-69-82-35-68;

E-mail address: Matthieu.Roy-Barman@lsce.ipsl.fr

Abstract

Sediment trap data are crucial for the study of marine biochemical cycles but they need careful validation by Thorium (Th) isotopes. In the present study, ^{230}Th, ^{232}Th, Uranium (U), Aluminum (Al), Barium (Ba) and Manganese (Mn) were analyzed in sinking particles collected by moored sediment traps in the Ligurian sea (DYFAMED site) in order to determine the collection efficiency of the traps and to constrain which particulate phase(s) carries Th isotopes in a region with strong lithogenic inputs. The $^{230}Th_{xs}$ evaluation was based on the U content of each sample rather than on the ^{232}Th content of each sample and the average $^{238}U/^{232}Th$ ratio of the continental crust because the latter method introduced too much uncertainty in the calculation. High trapping efficiencies (187 ± 85 % at 200 m and 87 ± 11 % at 1000 m) indicated no evidence of particle under-collection by the traps. The lack of correlation between $^{230}Th_{xs}$ and the carbonate or the organic matter fraction suggests that these phases are not major $^{230}Th_{xs}$-carrying phases in the deep ocean. For most samples of the time series, the $^{230}Th_{xs}$ concentration is correlated with the lithogenic fraction and the Mn concentration, but pulses of particles with high lithogenic and Mn content and low $^{230}Th_{xs}$ concentration occur in winter. Assuming that $^{230}Th_{xs}$ is only carried by lithogenic particles, we estimate $K_{d\_litho}{}^{Th}$ ranges from (0.42 ± 0.04) × 10^7 ml/g to (0.8 ± 0.2) × 10^7 ml/g. Assuming that $^{230}Th_{xs}$ is only carried by authigenic Mn oxide precipitates (MnO_2), we estimate that $K_{d\_MnO2}{}^{Th}$ ranges from (0.6 ± 0.1) × 10^{10} ml/g to (1.1 ± 0.4) × 10^{10} ml/g. The relative variation of $K_{d\_MnO2}{}^{Th}$ (a factor 7) between different oceanic sites is significantly lower than the relative variation of $K_{d\_litho}{}^{Th}$ (a factor 50), suggesting that $^{230}Th_{xs}$ has a tighter link with MnO_2 rather than with lithogenic particles and hence that $^{230}Th_{xs}$ may be more likely scavenged by MnO_2 than by lithogenic particles. The unambiguous determination of the particles carrying $^{230}Th_{xs}$ remains to be done.

Keywords: thorium, scavenging, sediment trap, trapping efficiency, marine particle, Mediterranean Sea, DYFAMED

1. Introduction

Understanding the oceanic carbon cycle requires reliable measurements of the particulate carbon fluxes in the ocean. More generally, the quantification of particulate fluxes is a cornerstone of the study of marine biogeochemical cycles. These fluxes are estimated with sediment traps. While sediment trap data are very limited spatially and temporally for logistical and financial reasons, they are critically important to tune the ocean biological pump in global biogeochemical models used to evaluate the fate of the carbon cycle (Usbeck et al., 2003). However, turbulence around the trap aperture can prevent a significant fraction of the sinking particles from being collected (Buesseler et al., 2007). Therefore, it is critical to validate sediment trap data. Uranium (U) - Thorium (Th) radioactive decay series are used to evaluate the efficiency of moored sediment traps (Bacon et al., 1985). ^{230}Th is produced uniformly in the ocean by radioactive decay of ^{234}U. Thorium is a very particle-reactive element, so that ^{230}Th is rapidly scavenged on sinking particles and transported toward the bottom of the ocean (Bacon and Anderson, 1982). If a trap works correctly, it should collect an average ^{230}Th sinking flux equal to the production of ^{230}Th by radioactive decay of ^{234}U above the trap. As the ^{230}Th flux collected by a sediment trap varies seasonally with the particle flux, annually averaged fluxes are considered in order to cancel seasonal variations of the ^{230}Th flux that reflect short-term departures from the longer-term steady state between production and removal of ^{230}Th (Bacon et al., 1985). Yearly averaged trapping efficiencies (the ratio between the trapped flux of ^{230}Th and the radioactive production) as low as 10% have been obtained in surface waters and in the mesopelagic zone (where horizontal currents are high) confirming that some traps largely undercollect the particles (Guieu et al., 2005; Scholten et al., 2001). Very different evolutions of the particle flux throughout the water column have been obtained when trapping efficiency corrections are used and when they are ignored (Guieu et al., 2005; Scholten et al., 2001; Yu et al., 2001). Sediment traps may also discriminate among different types of particles, with large and rapidly sinking particles expected

to be collected more efficiently into the traps than small and slowly sinking particles (Buesseler et al., 1992). Therefore, a Th–based trapping efficiency may not be relevant for all particles and compounds collected by the traps. Similar potential difficulties exist in paleo-oceanography with the determination of sedimentary focussing/winnowing factors by the ^{230}Th-normalisation method (Adkins et al., 2006; Francois et al., 2004). Thus, the determination of the phase(s) carrying Th isotopes is a key issue.

One way to address this question is to consider the correlations of ^{230}Th with the major phases (carbonate, biogenic silica, lithogenic particles, organic matter) constituting the particles compositions (Chase and Anderson, 2004; Chase et al., 2002; Luo and Ku, 2004a; Luo and Ku, 2004b; Roy-Barman et al., 2005; Scholten et al., 2005). However, this method suffers from multiple correlations between the different components of the marine particles producing spurious correlations between ^{230}Th and some phases unrelated with ^{230}Th scavenging, so that the result remains controversial. A recent work has highlighted the possible role of minor phases such as Manganese (Mn) oxides on ^{230}Th scavenging (Roy-Barman et al., 2005). However, it was based on a limited dataset that did not include samples with very high concentration in lithogenic particles. Here, we present a set of sediment trap data obtained at the DYFAMED site in the Ligurian Sea. This site receives sporadically a heavy load of Saharan dust particles and the particle dynamics are particularly well documented (Migon et al., 2002). Hence, this data set gives a good opportunity to test the Mn hypothesis in a lithogenic-rich environment. It was also the opportunity to evaluate the collection efficiency of the traps at this site: while the DYFAMED (DYnamique des Flux Atmosphériques en MEDiterranée) time series was started in 1987, this evaluation has not been done yet.

2. Sampling and analytical methods

2.1. Trap deployment

The DYFAMED station (Fig. 1) is located in the western basin of the Mediterranean Sea, 30 nautical miles (54 km) off Nice (43°25 N - 07°54 E, water depth: 2330 m). Sinking particulate matter was collected at 200 m and 1000 m from July 1999 to July 2000 as part of the DYFAMED sediment trap time series. The traps were multisampling conical sediment-traps (Technicap PPS5) with a collection surface of 1 m^2. Sampling cups were poisoned with formaldehyde prior to trap deployment in order to prevent grazing in the traps. The sampling interval was of 7 days, but in order to reduce the number of analyses, composite samples were prepared with sampling steps ranging from 7 to 35 days (a higher temporal resolution was used during high flux periods).

2.2. Analysis of particulate phases

Sampling procedures followed the JGOFS protocols and can be found elsewhere (Miquel et al., 1994). Back in the laboratory, swimmers were removed from the samples. The whole sample was then rinsed with ultra pure (MilliQ) and freeze-dried. Concentrations of total (TC) and organic (POC) carbon were measured in Monaco in triplicates with a Vario-El CHN elemental microanalyzer on aliquots of the desiccated samples. Aliquots of approximately 20 mg of the desiccated samples were digested in acid (HNO_3 + HF). Digestions were performed in a pressure-assisted microwave oven. For all the acid-digested samples Barium (Ba) was analyzed by quadrupole ICP-MS (Perkin Elmer Elan 6000, LEGOS, Toulouse). Aluminum (Al), Mn and U concentrations were determined by quadrupole ICP-MS (ThermoElectron XseriesII, LSCE, Gif sur Yvette).

Details on the material collected by the traps can be found at http:/www.obs-vlfr.fr/sodyf/. Trapped particles are mainly composed of marine snow, detritus, fecal pellets and lithogenic particles in variable proportions. The fraction of aluminosilicate is given by $f_{litho} = (11.1 \pm 1.1) \times Al$ (in g/g). It

corresponds to an Al content (9 ± 1) % in the insoluble fraction of Saharan dusts of different origins (Avila et al., 2007). The carbonate fraction was determined from Particulate Inorganic Carbon (PIC) as follows: $f_{CaCO3} = 8.3 \times PIC$ by assuming that all PIC is associated to $CaCO_3$. The organic matter content is assumed to be twice the POC content: $f_{om} = 2 \times POC$ (Klaas and Archer, 2002). Biogenic silica is known for not being a major ^{230}Th scavenging phase in trapped material (Chase et al., 2002; Roy-Barman et al., 2005). Therefore, it will not be considered in the following discussion. Excess Ba (Ba_{ex}) was used to evaluate the abundance of biogenic Ba (Sternberg et al., 2007). It was obtained by subtracting a Ba lithogenic fraction estimated with the Al content of the trapped material and a Ba/Al ratio of $(6.7 \pm 1.0)\times10^{-3}$ g/g that corresponds to the insoluble fraction of Saharan dusts (Avila et al., 2007). Mn was measured to evaluate the abundance of Mn oxides. The authigenic Mn fraction (Mn_{auth}) was obtained by subtracting a lithogenic fraction estimated with the Al content of the trapped material and a Mn/Al ratio of $(8.5 \pm 0.5)\times10^{-3}$ g/g that corresponds to the insoluble fraction of Saharan dusts (Avila et al., 2007).

2.3. Analysis of ^{230}Th and ^{232}Th

^{230}Th and ^{232}Th were analyzed on an aliquot of the same solution obtained for major and trace elements (see above). ^{229}Th spike was added to this aliquot. After isotopic equilibration, the Th was purified by ion exchange chemistry (Roy-Barman et al., 1996). Procedural blanks (around 20 pg of ^{232}Th and 0.1 fg of ^{230}Th) represent typically less than 1-2 % of the Th mass in the samples. The samples were analyzed in Toulouse by MC-ICP-MS on a Neptune (Finnigan) instrument following a procedure described previously (Guieu et al., 2005; Roy-Barman et al., 2005). The agreement between the measured $^{230}Th/^{232}Th$ ratio and the recommended value (Banner et al., 1990) of a Th standard indicates that the accuracy of the MC-ICP-MS measurement is typically better than 2%.

3. Results

The ^{232}Th concentration ranges from 0.90 ± 0.01 ppm to 9.9 ± 0.2 ppm at 200 m and from 4.30 ± 0.02 ppm to 9.4 ± 0.1 ppm at 1000 m (Tab.1). The ^{230}Th concentration ranges from 4.9 ± 0.3 pg/g to 46.3 ± 0.7 pg/g at 200 m and from 28.8 ± 0.6 pg/g to 47.0 ± 0.6 pg/g at 1000 m (Tab.1).

The ^{230}Th produced by *in situ* decay of dissolved ^{234}U and that is scavenged on particles ($^{230}Th_{xs}$) is often calculated by subtracting the lithogenic ^{230}Th component to the total ^{230}Th:

$$^{230}Th_{xs} = {}^{230}Th_{measured} - {}^{232}Th_{measured} \times (^{230}Th/^{232}Th)_{litho} \quad (1)$$

In previous studies of Th isotopes in the Mediterranean sea (Arraes-Mescoff et al., 2001; Roy-Barman et al., 2002), a ratio $(^{230}Th/^{232}Th)_{litho} = 4.4 \times 10^{-6}$ mol/mol was used based on a mean composition of the continental crust (Andersson et al., 1995). However, in the present study, we have analyzed samples with $(^{230}Th/^{232}Th)$ as low as $(4.0 \pm 0.1) \times 10^{-6}$ mol/mol at 200 m in winter (sample 7B). This indicates that the value $(^{230}Th/^{232}Th)_{litho} = 4.4 \times 10^{-6}$ mol/mol used in these earlier works is too high because a negative $^{230}Th_{xs}$ obtained with equation 1 would have no physical meaning. The $^{230}Th/^{232}Th$ ratio of the lithogenic material ranges typically from 3.2×10^{-6} to 5.4×10^{-6} mol/mol (Anderson et al., 1990). The $^{230}Th/^{232}Th$ ratio of aerosols collected in Monaco ranges from $(4.6 \pm 0.1) \times 10^{-6}$ to $(7.4 \pm 0.1) \times 10^{-6}$ mol/mol (Pham et al., 2005). Using these average values to correct for the lithogenic ^{230}Th would also produce negative $^{230}Th_{xs}$ for numerous samples.

Alternatively, $^{230}Th_{xs}$ can be determined if the lithogenic U content ($^{238}U_{litho}$) of the sample is known, assuming that in this lithogenic material ^{230}Th should be at secular equilibrium with ^{234}U and ^{238}U (supported ^{230}Th):

$$^{230}Th_{xs} = {}^{230}Th_{measured} - {}^{238}U_{litho} \times (\lambda_{230Th} * m_{230Th}) / (\lambda_{238U} * m_{238U}) \quad (2)$$

where λ_{230Th} (= 9.24×10^{-6} y^{-1}) and λ_{238U} (1.55×10^{-10} y^{-1}) are the time constants for the radioactive decay of ^{230}Th and ^{238}U and m_{230Th} and m_{238U} their molar masses (this calculation neglects ^{235}U whose abundance is less that 1%). The hypothesis of the secular equilibrium between ^{230}Th and ^{238}U is necessary to use equation 1 and equation 2, although it is not always fulfilled in weathered lithogenic detritus (Pham et al., 2005). Further work is needed to precisely constrain the average $^{230}Th/^{238}U$ ratio of atmospheric aerosols particularly in areas dominated by these inputs.

The U content of the trapped sample ranges from 0.24 ± 0.25 ppm to 2.02 ± 0.06 ppm. The U content in crustal rocks ranges from 1 ppm (lower crust) to 2.8 ppm (upper crust) and hence atmospheric dust have variable U content (Taylor and McLennan, 1995). Organic matter is enriched in U at ppm level, whereas pelagic carbonates are depleted in U (< 0.1 ppm) (Anderson, 1982; Henderson and O'Nions, 1995). Therefore, a significant fraction of the U present in the sample could be authigenic U recently incorporated in organic matter. This authigenic U must not be taken into account to evaluate the supported ^{230}Th. Therefore, U_{litho} is bracketed with 2 extreme assumptions:

1) All the U in the trapped material is lithogenic and no correction of authigenic contribution has to be done ($U_{auth} = 0$):

$$U_{litho} = U_{measured} \quad (3)$$

2) Some U is lithogenic and an authigenic U fraction is associated to organic matter (and to organic matter only). To estimate the authigenic U concentration in organic matter, we normalise the total U concentration and the lithogenic fraction by the fraction represented by the lithogenic and organic material ($f_{litho} + f_{om}$):

$$U_{norm} = U/(f_{litho} + f_{om}) \quad (4)$$

$$f_{litho\text{-}norm} = f_{litho} /(f_{litho} + f_{om}) \quad (5)$$

This normalisation removes the dilution effect of U-poor phases (carbonates). In a diagram U_{norm} versus $f_{litho\text{-}norm}$, the U_{norm} value for $f_{litho\text{-}norm} = 0$ gives U_{om}, the authigenic U concentration in the organic matter (Fig. 2). It appears that $U_{om} \approx 0.5\text{-}1.5$ ppm. To maximize the authigenic U correction, we take $U_{om} = 1.5$ ppm. The authigenic U content of each sample is given by:

$$U_{auth} = U_{om} \times f_{om} \quad (6)$$

With the 2 limiting cases, the mean U_{litho} and the range of uncertainty on the value are:

$$U_{litho} = U_{measured} - U_{auth}/2 \pm (U_{auth}/2 + \text{error on } U_{measured}) \quad (7)$$

The $U_{measured}$ value is the upper bound of this range. We note that the analytical uncertainty on $U_{measured}$ is small compared to the uncertainty introduced by the 2 limiting cases. In future studies, the analysis of the $^{234}U/^{238}U$ ratio could contribute to further constrain the nature of U in marine particles and sediments.

The $^{230}Th_{xs}$ is then given by equation 2. The $^{230}Th_{xs}$ concentration ranges from - 0.6 ± 1.8 pg/g to 19.1 ± 2.4 pg/g at 200 m and from 2.8 ± 2.1 pg/g to 21.3 ± 2.6 pg/g at 1000 m (Tab. 1). The highest $^{230}Th_{xs}$ concentrations are generally found in the deepest traps in summer whereas the $^{230}Th_{xs}$ concentrations are low in winter. On average, $^{230}Th_{xs}$ represents 28 % of the total ^{230}Th at 200 m and between 35% of the total ^{230}Th at 1000 m.

4. Discussion

4.1. Particle dynamics at the DYFAMED site

4.1.1. Temporal evolution and control of the particle flux

Despite its proximity to the continent, the DYFAMED site is considered as an “open ocean” site because it is protected from direct inputs of coastal waters by the Ligurian current (Marty et al., 2002). The Saharan dusts reaching DYFAMED have travelled at least 1000 or 2000 km since they

have left their desert sources. As a consequence, the lithogenic material found at the DYFAMED site is characteristic of eolian material rather than of direct river inputs. Hence, the temporal variability of the particle concentration and flux is due to local forcing rather than to advective inputs (Stemmann et al., 2002). The vertical particule flux is influenced by the biological production (regulated by the vertical inputs of nutrients), the atmospheric dust inputs of Saharan and European origin and winter mixing (Miquel et al., 1994).

The fate of the atmospheric dusts deposited at DYFAMED deserves attention because it will be used in the discussion in section 4.2.3. The deposition of Saharan dust over the Mediterranean Sea occurs mostly in spring and summer although strong pulses may also occur in winter (Migon et al., 2002). This general pattern can be compared with the total atmospheric deposition of Al recorded from July 1999 to July 2000 at the Pirio site on the NW coast of Corsica (Loÿe-Pilot et al., 2001). This site located 240 km SE of DYFAMED (Fig. 1) is free of local contamination and the atmospheric fluxes recorded at Pirio are consistent with those collected on the French Riviera (Loÿe-Pilot et al., 2001). Therefore, it represents a good recording of the Saharan dust deposition events that are susceptible to have reached DYFAMED. At Pirio, strong Al deposition from July to October 1999 (1.25-9.24 mg/m^2/d) and from Mid-April to July 2000 (1.20-3.67 mg/m^2/d), whereas very low fluxes are recorded from November 1999 to Mid-April 2000 (0.03-0.16 mg/m^2/d) (Fig. 3). This lack of Saharan events during this period was also observed over the same period at the La Castanya Biological Station (NE Spain)), where no red rain event was recorded from November 15th 1999 to March 25th 2000 (Avila et al., 2007).

The vertical Al flux recorded at DYFAMED at 200 m are clearly not synchronized with the atmospheric deposition described above (Fig. 3). From July 15th 1999 to December 5th 1999, the Al

231 flux trapped at 200 m is always lower than 1.5 mg/m^2/d, whereas from December 9th 1999 to June 25th
232 2000, it ranges from 4.9 mg/m^2/d to 16.9 mg/m^2/d.

233 In previous studies, the vertical transfer of marine particles at the DYFAMED site was
234 described as a three step seasonal transfer scenario (Migon et al., 2002; Sarthou and Jeandel, 2001;
235 Sicre et al., 1999; Ternois et al., 1996) that accounts for the observations presented above:
236 (i) In summer and autumn, during the period of water stratification, biological fluxes are low and do
237 not allow the transfer of lithogenic material down to 200 m depth. Atmospheric material accumulates
238 along the seasonal thermocline, while below the thermocline a series of physico-chemical processes
239 lead to the formation of small non-biogenic aggregates. During that period, the residence time of the
240 suspended particles is the surface water can exceed 200 days (Schmidt et al., 2002).
241 (ii) In winter, the disappearance of the thermocline (and the sinking of dense water when it occurs) is
242 responsible for a rapid downward transfer of the lithogenic matter accumulated in the surface layer.
243 (iii) In spring, the availability of nutrients brought to surface waters by the winter vertical mixing
244 allows phytoplankton blooms. The sinking of particulate matter (including atmospheric dust) is then
245 governed by biological activity and can be very fast (Buat-Ménard et al., 1989; Fowler et al., 1987;
246 Schmidt et al., 1992).

247 Due to the lack of sedimentation between the end of the summer bloom and the winter mixing,
248 the lithogenic rich particles collected at 200 m or 1000 m in winter have spent several (3-5) months
249 above and at the seasonal thermocline. This is less than the residence time estimated for the suspended
250 particles between the surface and 200 m or 1000 m. At DYFAMED, the mean settling speed of the
251 small (> 0.2 μm) particle estimated by the $^{230}Th_{xs}$ method is S = 250 m/y (Roy-Barman et al., 2002).
252 This settling speed of small particles is in the lower end of the range determined in the ocean. In the
253 oligotrophic Central North Pacific, the small particle settling speed is of 330 m/y (Roy-Barman et al.,

1996) whereas in coastal areas the settling speed is of the order of 1000 m/y (Huh and Beasley, 1987). The estimate of the settling speed at DYFAMED (Roy-Barman et al., 2002) may not be very accurate because it is based on a budget that depends more on the ventilation rate of the deep waters than on the thorium scavenging rate. Therefore, we suspect that this value underestimates the true settling speed. Hence, the mean settling time of the suspended particles is expected to be less than 1 year between 0 and 200 m and of the order of 3 years between 200 m and 1000 m.

The particles collected at 200 m or 1000 m are not simply surface-derived particles. Their chemical composition is affected by the mineralization of organic compounds (Sempéré et al., 2000), by the dissolution of inorganic elements (Arraes-Mescoff et al., 2001) and aggregation of suspended particles (Roy-Barman et al., 2002, Coppola et al., 2006). Aggregation is best visible by the increase of the $^{230}Th_{xs}$ flux between 200 m (0.24 ± 0.11 pg/m^2/y) and 1000 m (0.56 ± 0.07 pg/m^2/y). It is likely that this increase of $^{230}Th_{xs}$ flux between 200 m and 1000 m is due to aggregation of suspended particles that are enriched in *in situ* produced ^{230}Th due to their high specific surface and long residence time in the water column rather than to direct adsorption of *in situ* produced ^{230}Th on trapped particles (Roy-Barman et al., 2002).

4.1.2. Sediment trap efficiency

It is worth evaluating the collection efficiency of the trap because a low efficiency can modify the chemical composition of the trapped material by, as an example, an under-sampling of the finest particles (Roy-Barman et al., 2005). To cancel the short-term seasonal variations of the $^{230}Th_{xs}$ flux induced by the seasonal variations of the particle flux, the annually averaged $^{230}Th_{xs}$ flux is considered (Bacon et al., 1985). Assuming that $^{230}Th_{xs}$ is transported vertically by the settling particles only, the collection efficiency (E) is just the ratio between the flux of $^{230}Th_{xs}$ collected by the trap during a full

277 year (F) and the quantity of $^{230}Th_{xs}$ produced over the trap by radioactive decay of ^{234}U (Guieu et al.,
278 2005):

279 $$E = \frac{F}{P \times h} \quad (8)$$

280

281 where F is the year-averaged $^{230}Th_{xs}$ flux collected by the trap, P is the ^{230}Th production rate (P = 0.65
282 fg/l/y in the salty Mediterranean sea) and h is the trap depth. Under these assumptions, we obtain E =
283 187 ± 85 % at 200 m and E = 87 ± 11 % at 1000 m.

284 Overall, the trapping efficiency is close to 100 % considering the uncertainties and there is no
285 evidence of strong under-trapping. This high trapping efficiency can be related to the generally low
286 speed of the currents at 200 m and 1000 m at DYFAMED (Miquel and La Rosa, 2001; Roy-Barman et
287 al., 2002). This is the first published determination of the PPS5 trap efficiency at DYFAMED and it
288 validates the numerous sediment trap based studies at DYFAMED.

289

290 *4.2. Testing the potential carriers of $^{230}Th_{xs}$*

291 In this section, we look at the correlations between the concentration of $^{230}Th_{xs}$ and of different
292 phases constituting the particulate material. With this approach of comparing concentrations rather
293 than vertical fluxes, we try to determine the phases on which $^{230}Th_{xs}$ is adsorbed but not necessarily
294 the ones that create the vertical flux through aggregation and ballasting. The parameters controlling
295 the partition coefficient $K_{d\_bulk}^{Th}$ between the bulk particulate and the dissolved phases are
296 controversial. Field-based estimate of $K_{d\_bulk}^{Th}$ is obtained by dividing the amount of nuclides per g of
297 bulk trapped particles by the total amount of nuclides (dissolved+particulate) per ml of seawater in the
298 water through which the particle sunk.

299 $K_{d\_bulk}^{Th} = [^{230}Th_{xs}]_{particulate\ matter}/[^{230}Th_{xs}]_{seawater}$ (9)

And for the fractionation between a given phase of the particulate matter and seawater:

$$K_{d\_phase}^{Th} = K_{d\_bulk}^{Th} / [phase]_{particulate\ matter} \quad (10)$$

In the southern and Pacific oceans, the correlation between $K_{d\_bulk}^{Th}$ and the carbonate content of trapped particles suggests that ^{230}Th scavenging is controlled by carbonates (Chase and Anderson, 2004; Chase et al., 2002; Chase et al., 2003). In regions with higher lithogenic content in the trapped material, both carbonate and lithogenic material should scavenge ^{230}Th (Chase et al., 2002; Narita et al., 2003). Revisiting the same data set, Luo and Ku (2004) noted a strong correlation between $K_{d\_bulk}^{Th}$ and the lithogenic content of the trapped particles and proposed that ^{230}Th is scavenged mainly by the lithogenic phase (Luo and Ku, 2004a; Luo and Ku, 2004b). However, the $K_{d\_litho}^{Th}$ (2.3×10^8 ml/g) obtained at these sites is more than one order of magnitude larger than those obtained in regions with strong lithogenic inputs (1×10^7 ml/g) (Chase et al., 2002). In the Arctic Ocean where biological productivity is very low, ice-rafted lithogenic particles are proposed to scavenge ^{230}Th (Edmonds et al., 1998; Trimble et al., 2004). In the Arabian Sea, the lack of consistency between $K_{d\_bulk}^{Th}$ and the major components of the sinking particles suggested that Th scavenging is not controlled by major phases (Scholten et al., 2005). More recently, it was proposed that Mn oxides rather than lithogenic particles or carbonates control ^{230}Th scavenging on marine particles (Roy-Barman et al., 2005). This was based on (1) the strong correlation between Mn and ^{230}Th content of marine particles collected in the NE Atlantic Ocean and (2) the consistency of the $K_{d\_MnO2}^{Th}$ estimates over a large range of oceanic environment. However, only a limited number of samples from area with strong lithogenic inputs were available in this study and we now re-explore the possible relationships between $^{230}Th_{xs}$ and the different components of the DYFAMED trapped particles.

321

322 *4.2.1. $CaCO_3$*

323 The lack of correlation between $CaCO_3$ and $^{230}Th_{xs}$ (Fig. 4a) is consistent with the results
324 obtained in the NE Atlantic and in the Arabian Sea (Roy-Barman et al., 2005; Scholten et al., 2005). It
325 confirms that the linear correlation observed between $CaCO_3$ and $^{230}Th_{xs}$ in the Southern Ocean and in
326 the Equatorial Pacific (Chase et al., 2002) is not a general feature. This correlation may be due to the
327 fortuitous correlation of $CaCO_3$ and $^{230}Th_{xs}$ bearing phases, possibly MnO_2 or lithogenic particles
328 (Roy-Barman et al., 2005).

329

330 *4.2.2. Particulate Organic Matter*

331 The lack of correlation between Particulate Organic matter (estimated through POC
332 concentration) and $^{230}Th_{xs}$ (Fig. 4b) is consistent with the results obtained in the NE Atlantic, in the
333 Southern Ocean, in the Equatorial Pacific and in the Arabian Sea (Chase et al., 2002; Roy-Barman et
334 al., 2005; Scholten et al., 2005). It suggests that in the deep ocean ^{230}Th is not scavenged significantly
335 by organic matter (Roy-Barman et al., 2005) contrary to what is probably the case in surface waters
336 (Coppola et al., 2002, Quigley et al., 2002).

337

338 *4.2.3. Lithogenic particles*

339 There is not a single correlation between $^{230}Th_{xs}$ and ^{232}Th (Fig. 4c). This is not surprising
340 because $^{230}Th_{xs}$ is scavenged from seawater, whereas ^{232}Th is mostly introduced in the ocean
341 imbedded in lithogenic particles (Adkins et al., 2006; Roy-Barman et al., 2002). This is reflected by
342 the high correlation between the ^{232}Th concentration and the Al concentration in the trapped material
343 (not shown, $R^2 = 0.98$). Most samples define a gross linear relationship between $^{230}Th_{xs}$ and ^{232}Th (200

m: R^2 = 0.87 and 1000 m: R^2 = 0.75). Lithogenic-rich samples collected during winter (and early spring) do not fall on the main trend (circles with a cross inside in Fig. 4).

A double correlation between $^{230}Th_{xs}$ and ^{232}Th was also obtained during the POMME experiment in the North Atlantic (Roy-Barman et al., 2005). The main correlation was explained by a mixture between small suspensions (enriched in ^{230}Th) and lithogenic particles, whereas winter samples with high ^{232}Th content and low $^{230}Th_{xs}$ where due to a rapid transfer at depth of atmospheric dust deposited at the sea surface (within 2 weeks at 400 m and the week after at 1000 m). This rapid transfer may have been due to incorporation of the dusts in faecal pellets or in marine snow. Therefore, it was not possible to determine if these samples where not enriched in $^{230}Th_{xs}$ because the $K_{d\_litho}^{Th}$ is low or because $^{230}Th_{xs}$ had not enough time to equilibrate with the newly arrived lithogenic particles and seawater.

The DYFAMED site offers the opportunity to tackle this question. As explained in section 4.1.1., the lithogenic particles deposited in summer and autumn are not transferred directly through the thermocline but rather stored at the top of the thermocline (during 3-5 months) until winter convection allow them to cross the thermocline. Then, it takes 2 additional months for the lithogenic particles to go from 200 m to 1000 m as indicated by the time lag of the Al flux between 200 m and 1000 m (Fig. 3). Despite this longer equilibration time between the lithogenic particles and seawater compared to the POMME data, the lithogenic rich samples plot below the main $^{230}Th_{xs}$ – lithogenic fraction correlation at both 200 m and 1000 m. The transit time of these particles is not as long as the average residence time of the bulk suspended particles in the water column (see section 4.1.1.). So it is possible that there was not enough time for $^{230}Th_{xs}$ to reach complete equilibration between the winter lithogenic particles and seawater. However, in the North Atlantic, the particles transporting a Saharan dust pulse at 1000 m within 3 weeks have a larger $K_{d\_litho}^{Th}$ than particles transporting a Saharan dust pulse in several months at 1000 m at DYFAMED. It suggests that the kinetic of ^{230}Th adsorption on

lithogenic particles is not the limiting factor of the ^{230}Th uptake by sinking particles. This is also consistent with in vitro experiments indicating a fast sorption of ^{230}Th on lithogenic particles (Geibert and Usbeck, 2004). Nevertheless, deposition of larger dust particles at DYFAMED compared to the North Atlantic could explain the lower affinity of ^{230}Th for DYFAMED particles due to their lower surface to volume ratio. Alternatively, it was proposed that the $^{230}Th_{xs}$ content of trapped particles is controlled by the incorporation of $^{230}Th_{xs}$-rich, Ba-rich and Mn-rich suspended particles to the rapidly sinking particles (Huang and Conte, 2009; Roy-Barman et al., 2005). This mixing would then control the apparent $K_{d\_litho}^{Th}$ of the trapped particles. The low Ba content of lithogenic-rich winter samples indicate a low contribution of the small suspended particle pool (Barite tend to accumulate in this small particle pool (Sternberg et al., 2007)) despite high lithogenic content. In any case, the DYFAMED results confirm that arrival of atmospheric pulses of Saharan material decreases the degree of correlation between the $^{230}Th_{xs}$ and f_{litho} for the whole dataset.

Assuming that all the $^{230}Th_{xs}$ is adsorbed on the lithogenic material and that there is a chemical equilibration of $^{230}Th_{xs}$ between lithogenic particles and seawater, we can estimate $K_{d\_litho}^{Th}$ with the trapped particles analyzed in the present work and seawater data (Roy-Barman et al., 2002). We focus on the 1000 m samples, because their $^{230}Th_{xs}$ is less sensitive to uncertainties on lithogenic correction and because there is some concern that at shallower depth the equilibration between seawater and particulate matter is not achieved (Chase et al., 2002). We obtain $K_{d\_litho}^{Th} = (0.7 \pm 0.2)\times10^7$ for the main trend samples and $K_{d\_litho}^{Th}$ $(0.36 \pm 0.04) \times 10^7$ for the winter samples (Tab. 2). These values are consistent with the result of $K_{d\_litho}^{Th} \approx 10^7$ obtained by (Chase et al., 2002) based on Atlantic samples and much lower than the value $K_{d\_litho}^{Th} \approx 23\times10^7$ estimated by (Luo and Ku, 2004a) based on sample collected in area experiencing very low eolian inputs.

390

391 *4.2.4. Mn oxides*

392 The relationship between $^{230}Th_{xs}$ and Mn is quite similar to the relationship between $^{230}Th_{xs}$
393 and the lithogenic fraction (Fig. 4c,e): excluding the winter samples, good correlations are obtained
394 between $^{230}Th_{xs}$ and Mn (200 m: $R^2 = 0.83$ and 1000 m: $R^2 = 0.86$). In the NE Atlantic, the lithogenic
395 content of the trapped particle was low enough (<10%) so that the lithogenic contribution to the total
396 Mn was generally less than 50 % and a good correlation was found between $^{230}Th_{xs}$ and Mn (Roy-
397 Barman et al., 2005). The winter samples are still not on the main trend on a $^{230}Th_{xs}$ and Mn_{auth}
398 diagram (fig 4f) and excluding the winter samples, the goodness of fit of the $^{230}Th_{xs}$ versus Mn_{auth} data
399 (200 m : $R^2 = 0.56$ and 1000 m: $R^2 = 0.69$) is not as good as the $^{230}Th_{xs}$ and Mn correlation. However,
400 correcting the DYFAMED samples for the lithogenic Mn contribution requires caution because the
401 Mn/Al ratio of the insoluble fraction of Saharan dusts $(8.5 \pm 0.5)\times10^{-3}$ g/g is variable (Avila et al.,
402 2007). In addition, the Mn/Al ratio of the "Saharan aerosols" collected in "clean" sites of Corsica or of
403 the French Riviera (Mn/Al = 16×10^{-3} - 38×10^{-3}) can be 3-4 times higher indicating the contribution of
404 an anthropogenic Mn source (possibly European aerosols) (Ridame et al., 1999). Finally, Mn
405 dissolution can occur when it enters seawater (Guieu et al., 1994) or during particulate organic matter
406 mineralization (Arraes-Mescoff et al., 2001).

407 The Mn/Al ratio of the DYFAMED samples range from 5×10^{-3} to 16×10^{-3} (average: 12.0×10^{-3})
408 at 200 m and from 11×10^{-3} to 18×10^{-3} (average: 13.4×10^{-3}) at 1000 m. These values are within the
409 range of the crustal rock average and at the low end of the atmospheric inputs range so that it is
410 difficult to correct for the "non authigenic" Mn fraction. The maximum of anthropogenic inputs
411 occurs at the end of summer (before winter mixing) and the end of winter (during winter mixing)
412 (Migon et al., 2008). Therefore, we cannot rule out that the Mn-rich and $^{230}Th_{xs}$-poor winter samples

fall out of the main correlation because the Mn/Al ratio of their dusts is larger than the value used to calculate Mn_{auth}.

In surface waters, photoreduction limits the formation of Mn oxides, so that particulate Mn is associated with organic matter (Johnson et al., 1996). Below the photic zone, Mn oxides are precipitated on marine particles throughout the water column (Huang and Conte, 2009; Johnson et al., 1996). Assuming that all the $^{230}Th_{xs}$ is adsorbed on these authigenic Mn oxides and that there is a chemical equilibration of $^{230}Th_{xs}$ between these oxides and seawater, we can estimate $K_{d\_MnO2}^{Th}$. Still focussing on the 1000 m samples, we obtain $K_{d\_MnO2}^{Th} = (1.1 \pm 0.4)\times10^{10}$ for the main trend samples and $K_{d\_MnO2}^{Th} = (0.6 \pm 0.1) \times 10^{10}$ for the winter samples (Tab. 2). These values are lower but grossly consistent with the result of $K_{d\_MnO2}^{Th} \approx 2 \times 10^{10}$ obtained for the Atlantic Ocean (Roy-Barman et al., 2005) and $K_{d\_MnO2}^{Th} \approx 3.5\times10^{10}$ estimated from sample collected in area experiencing very low eolian inputs (Luo and Ku, 1999; Roy-Barman et al., 2002).

In the previous section and in the present one, we successively assumed that all the $^{230}Th_{xs}$ is carried by the lithogenic particles or by the authigenic Mn oxides. We now try to choose between these 2 hypotheses. It is well established that the slope of the correlation between the $^{230}Th_{xs}$ concentration and the lithogenic fraction of trapped particles is site-dependent (Chase and Anderson, 2004; Chase et al., 2002; Luo and Ku, 2004a; Luo and Ku, 2004b; Roy-Barman et al., 2005). Much of the controversy on affinity of $^{230}Th_{xs}$ for lithogenic particles resides in the interpretation of this site-dependent slope that may reflect (1) true variations of $K_{d\_litho}^{Th}$ from one site to the other depending on the chemical and size characteristics of the lithogenic particles (Luo and Ku, 2004a; Luo and Ku, 2004b) or (2) more or less fortuitous correlation between the lithogenic fraction and another phase by which the $^{230}Th_{xs}$ is effectively taken up such as carbonates (Chase and Anderson, 2004; Chase et al., 2002) or Mn oxides (Roy-Barman et al., 2005). The present study does not allow choosing clearly

between the 2 hypotheses because the Mn concentration and the lithogenic fraction are strongly correlated (R^2=0.92). However, we note that if neither $K_{d\_litho}^{Th}$ nor $K_{d\_MnO2}^{Th}$ are constant between high dust and low dust sites, $K_{d\_MnO2}^{Th}$ estimated from sediment trap data varies by at most a factor 7, whereas $K_{d\_litho}^{Th}$ varies by a factor 50 (Tab. 2). Thus the affinity of $^{230}Th_{xs}$ for Mn oxides appears to be much less "site-dependent" than its affinity for lithogenic particles, suggesting a stronger link between $^{230}Th_{xs}$ scavenging and authigenic MnO_2 precipitation than with lithogenic particles. In that case lithogenic matter may serve as support for Mn oxide precipitation and then as ballast for its transport.

These results combined with the lack of correlation found between the $^{230}Th_{xs}$ concentration and the $CaCO_3$ content of trapped particles at DYFAMED as well as in previous studies (Roy-Barman et al., 2005; Scholten et al., 2005), suggests that the high $K_{d\_CaCO3}^{Th}$ used in various modelling studies (Dutay et al., 2009; Siddall et al., 2005) should be re-evaluated and that Mn coatings have to be taken into account in these models. The correlation between $^{230}Th_{xs}$ and carbonates at some sites could be explained if carbonates are substrates for Mn oxide precipitation (Martin and Knauer, 1983).

5. Conclusion

The present study brings a new insight on thorium scavenging in regions with strong lithogenic inputs. The lack of correlation between $^{230}Th_{xs}$ and the carbonate and organic matter fractions suggests that carbonates and organic matter are not the main phases carrying the in situ ^{230}Th in the Mediterranean Sea. The high temporal resolution of DYFAMED sediment trap time series indicates that different correlations exist between $^{230}Th_{xs}$ concentration and the lithogenic fraction of the trapped particles. Most samples define a correlation between $^{230}Th_{xs}$ and the lithogenic fraction but lithogenic-rich and $^{230}Th_{xs}$ – poor particle pulses occur in winter. Assuming that $^{230}Th_{xs}$ is only carried

by lithogenic particles, the estimated value of $K_{d\_litho}^{Th}$ range from (0.42 ± 0.04) × 10^7 ml/g to (0.8 ± 0.2) × 10^7 ml/g. Similarly, a correlation between the $^{230}Th_{xs}$ concentration and the Mn concentrations occurs with also Mn-rich and $^{230}Th_{xs}$ – poor particle pulses in winter. Assuming that $^{230}Th_{xs}$ is only carried by authigenic MnO_2 precipitates, the estimated value of $K_{d\_MnO2}^{Th}$ ranges from (0.6 ± 0.1) × 10^{10} ml/g to (1.1 ± 0.4) × 10^{10} ml/g. Comparing K_d^{Th} obtained at different sites indicates that the range of variation of $K_{d\_MnO2}^{Th}$ is significantly lower than the range of variation $K_{d\_litho}^{Th}$, suggesting that $^{230}Th_{xs}$ has a tighter link with MnO_2 rather than with lithogenic particles and that hence MnO_2 is a more likely carrier of $^{230}Th_{xs}$ than lithogenic particles. The unambiguous determination of the particles carrying thorium isotopes remains to be done.

Acknowledgments

We warmly thank J.-C. Marty, PI of the DYFAMED program until 2007, for his support. We are grateful to R. Freydier for his help with the Neptune utilization and to F. Candaudap for his help with the Elan 6000 utilization. Discussions with M.-A. Sicre, C. Guieu and L. Coppola helped us to clarify our ideas about particle dynamics at DYFAMED. The thoughtful comments of W. Geibert, S. Luo and of an anonymous reviewer profoundly improved the article. The DYFAMED Program was supported by the French agencies CNRS/ INSU (PROOF-PATOM). The International Atomic Energy Agency is grateful for the support provided to its Marine Environment Laboratories by the Government of the Principality of Monaco.This is LSCE contribution number LSCE 3906.

Figure Captions

Figure 1: The DYFAMED station, in the western Mediterranean (from Ocean Data View)

Figure 2: U_{norm} versus f_{litho_norm}. See text for definitions. The straight lines represent mixing lines between hypothetical (lithogenic free) organic matter end members and lithogenic end members. It suggests that the organic matter end-member contains at most 1.5 ppm of authigenic U. Crustal end-member from (Taylor and McLennan, 1995).

Figure 3: Temporal evolution of the trapped material at 200 m and 1000 m and atmospheric deposit at Pirio in Corsica. A: Mass flux. B: Al flux.

Figure 4: $^{230}Th_{xs}$ as a function of the particle composition. a: $^{230}Th_{xs}$ versus $CaCO_3$. b: $^{230}Th_{xs}$ versus organic matter. c: $^{230}Th_{xs}$ versus lithogenic matter d: $^{230}Th_{xs}$ versus Ba_{xs}. e: $^{230}Th_{xs}$ versus Mn_{total}. f: $^{230}Th_{xs}$ versus Mn_{auth}. Large error bars on the lithogenic fraction, Ba_{xs} and Mn_{auth} are due to the variability of the composition of the insoluble fraction of Saharan aerosols (Avila et al., 2007).

References

Adkins J., deMenocal P., and Eshel G., 2006. The ‘‘African humid period’’ and the record of marine upwelling from excess 230Th in Ocean Drilling Program Hole 658C. Paleocanogr. 21, doi:10.1029/2005PA001200.

Anderson R. F., 1982. Concentration, vertical flux, and remineralisation of particulate uranium in seawater. Geochim. Cosmochim. Acta 46, 1293-1299.

Anderson, R. F., Bacon, M. P. and Brewer P. G., 1983. Removal of ^{231}Pa and ^{230}Th at ocean margins, Earth Planet. Sci. Lett. 66, 73-90.

Anderson R. F., Lao Y., Broecker W. S., Trumore S. E., Hofmann H. J., and Wolfli W., 1990. Boundary scavenging in the Pacific Ocean: a comparison of ^{10}Be and ^{231}Pa. Earth Planet. Sci. Lett. 96, 287-304.

Andersson P. S., Wasserburg G. J., Chen J. H., Papanastassiou D. A., and Ingri J., 1995. ^{238}U-^{234}U and ^{232}Th-^{230}Th in the Baltic sea and in river water. Earth Planet. Sci. Lett. 130, 217-234.

Arraes-Mescoff R., Coppola L., Roy-Barman M., Souhaut M., Tachikawa K., Jeandel C., Sempéré R., and Yoro C., 2001. The behavior of Al, Mn, Ba, Sr, REE and Th isotopes during *in vitro* bacterial degradation of large marine particles. Mar. Chem. 73, 1-19.

Avila A., Alarcon M., Castillo S., Escudero M., Garcia Orellana J., Masque P., and Querol X., 2007. Variation of soluble and insoluble calcium in red rains related to dust sources and transport patterns from North Africa to northeastern Spain. J. Geophys. Res. 112, doi:10.1029/2006JD007153.

Bacon M. P. and Anderson R. F., 1982. Distribution of thorium isotopes between dissolved and particulate forms in the Deep-Sea. J. Geophys. Res. 87, 2045-2056.

534 Bacon M. P., Huh C.-H., Fleer A. P., and Deuser W. G., 1985. Seasonality in the flux of natural
535 radionuclides and plutonium in the deep Sargasso Sea. Deep-Sea Res. 32, 273-286.
536 Banner J. L., Wasserburg G. J., Chen J. H., and Moore C. H., 1990. ^{234}U-^{238}U-^{230}Th-^{232}Th systematics
537 in saline groundwaters from central Missouri. Earth Planet. Sci. Lett. 101, 296-312.
538 Buat-Ménard P., Davies J., Remoudaki E., Miquel J. C., Bergametti G., Lambert C. E., Ezat U.,
539 Quetel C., La Rosa J., and Fowler S. W., 1989. Non steady state removal of atmospheric particles
540 from Mediterranean surface waters. Nature 340, 131-134.
541 Buesseler K. O., Antia A. N., Chen M., Fowler S. W., Gardner W. D., Gustaffson Ö., Harada K.,
542 Michaels A. F., Rutgers van der Loeff M., Sarin M., Steinberg D. K., and Trull T., 2007. An
543 assessment of the use of sediment traps for estimating upper ocean particle fluxes. J. Mar. Res.
544 65, 345-416.
545 Buesseler K. O., Bacon M., Cochran J. K., and Livingston H. D., 1992. Carbon and nitrogen export
546 during the JGOFS North Atlantic Bloom Experiment estimated from ^{234}Th:^{238}U desiquilibria.
547 Deep Sea Res. 39, 1115-1137.
548 Chase Z. and Anderson R. F., 2004. Comment on ‘‘On the importance of opal, carbonate, and
549 lithogenic clays in scavenging and fractionating ^{230}Th, ^{231}Pa and ^{10}Be in the ocean’’ by S. Luo
550 and T.-L. Ku. Earth Planet. Sci. Lett. 220, 213-222.
551 Chase Z., Anderson R. F., Fleisher M. Q., and Kubik P. W., 2002. The influence of particle
552 composition and particle flux on scavenging of Th, Pa and Be in the ocean. Earth Planet. Sci
553 Lett. 204, 215-229.
554 Chase Z., Anderson R. F., Fleisher M. Q., and Kubik P. W., 2003. Scavenging of ^{230}Th, ^{231}Pa and ^{10}Be
555 in the Southern Ocean(SW Pacific sector): the importance of particle flux, particle composition
556 and advection. Deep-Sea Res. II 50, 739–768.

557 Coppola, L., Roy-Barman, M., Mulsow, S., Povinec, P. and Jeandel, C., 2006. Thorium isotopes as
558 tracers of particles dynamics and deep water circulation in the Indian sector of the Southern
559 Ocean (ANTARES IV). Mar. Chem. 100, 299–313.
560 Coppola, L., Roy-Barman, M., Wassmann, P. and Jeandel, C., 2002. Calibration of sediment traps and
561 particulate organic carbon export using 234Th in the Barents Sea. Mar. Chem. 80, 11–26.
562 Dutay J.-C., Lacan F., Roy-Barman M., and Bopp L., 2009. Study of the influence of the particles'
563 size and type on the simulation of ^{231}Pa and ^{230}Th with a global coupled biogeochemical- ocean
564 general circulation model: a first approach. G3 10, doi:10.1029/2008GC002291.
565 Edmonds H. N., Moran S. B., Hoff J. A., Smith J. N., and Edwards R. L., 1998. Protactinium-231 and
566 Thorium-230 abundances and high scavenging rates in the Western Arctic Ocean. Science 280,
567 405– 407.
568 Fowler S. W., Buat-Ménard P., Yokohama Y., Ballestra S., Holm E., and Van Nguyen H. V., 1987.
569 Rapid removal of Chernobyl fallout from Mediterranean surface waters by biological activity.
570 Nature 329, 56-58.
571 Francois R., Frank M., Rutgers van der Loeff M. M., and Bacon M. P., 2004. 230Th normalization:
572 An essential tool for interpreting sedimentary fluxes during the late Quaternary.
573 Paleoceanography 19, PA1018, doi:10.1029/2003PA000939,.
574 Geibert W. and Usbeck R., 2004. Adsorption of thorium and protactinium onto different particle
575 types: Experimental findings. Geochim. Cosmochim. Acta 68, 1489–1501.
576 Guieu C., Duce R. A., and Arimoto R., 1994. Dissolved input of Manganese in the ocean: the aerosol
577 source. J. Geophys. Res. 99, 18789-18800.
578 Guieu C., Roy-Barman M., Leblond N., Jeandel C., Souhaut M., Le Cann B., Dufour A., and Bournot
579 C., 2005. Vertical particle flux in the North-East Atlantic Ocean (POMME experiment). J.
580 Geophys. Res. 110., doi:10.1029/2004JC002672.

Henderson G. and O'Nions R. K., 1995. 234U/238U ratios in quaternary planctonic foraminifera. Geochim. Cosmochim. Acta. 56(4685-4694).

Huang S. and Conte M. H., 2009. Source/process apportionment of major and trace elements in sinking particles in the Sargasso sea. Geochim. Cosmochim. Acta 73, 65–90.

Huh C.-A. and Beasley T. M., 1987. Profiles of dissolved and particulate thorium isotopes in the water column of coastal Southern California. Earth Planet. Sci. Lett. 85, 1-10.

Johnson K. S., Coale K. H., Berelson W. M., and Gordon R. M., 1996. On the formation of the manganese maximum in the oxygen minimum. Geochim. Cosmochim. Acta 60(8), 1291-1299.

Klaas C. and Archer D. E., 2002. Association of sinking organic matter with various types of mineral ballast in the deep sea: Implications for the rain ratio. Global Biogeochem. Cycles. 16, Art. No. 1116.

Kuss J. and Kremling K., 1999. Particulate trace element fluxes in the deep northeast Atlantic Ocean, Deep-Sea Res. I 46, 1377– 1403.

Loÿe-Pilot M. D., Guieu C., and Ridame C. (2001) Atmospheric bulk fluxes of natural and polluant metals to the North Western Mediteranean: Their trend over the last 15 years (1985-2000). In *UNEP/MAP/MEDPOL: Atmospheric Transport and Deposition of Pollutants into the Mediterranean Sea: Final Reports on Research Projects. MAP Technical Reports Series No. 133, UNEP/MAP, Athens, 2001*.

Luo S. and Ku T.-L., 1999. Oceanic $^{231}Pa/^{230}Th$ ratio influenced by particle composition and remineralisation. Eath Planet. Sci. Lett. 167, 183-195.

Luo S. and Ku T.-L., 2004a. On the importance of opal, carbonate and lithogenic clays in scavenging and fractionating ^{230}Th, ^{231}Pa and ^{10}Be in the ocean,. Earth Planet. Sci. Lett. 220, 201-211.

603 Luo S. and Ku T.-L., 2004b. Reply to Comment on ‘‘On the importance of opal, carbonate, and
604 lithogenic clays in scavenging and fractionating ^{230}Th, ^{231}Pa and ^{10}Be in the ocean’’. Earth
605 Planet. Sci. Lett. 220, 223-229.
606 Martin J. H. and Knauer G. A., 1983. Vertex: Manganese transport with CaCO3. Deep-Sea Res. 30,
607 411-425.
608 Marty J. C., Chiaverini J., Pizay M. D., and Avril B., 2002. Seasonal and interannual dynamics of
609 nutrients and phytoplankton pigments in the western Mediterranean Sea at the DYFAMED time-
610 series station (1991-1999). Deep Sea Res. II 49, 1965-1985.
611 Migon C., Robin T., Dufour A., and Gentili B., 2008. Decrease of lead concentrations in the Western
612 Mediterranean atmosphere during the last 20 years. Atmospheric Environment 42, 815–821.
613 Migon C., Sandroni V., Marty J.-C., Gasser B., and Miquel J.-C., 2002. Transfer of atmospheric
614 matter through the euphotic layer in the northwestern Mediterranean: seasonal pattern and
615 driving forces. Deep-Sea Res. II 49, 2125–2141.
616 Miquel J. C., Buat-Ménard P., Fowler S. W., and La Rosa J., 1994. Dynamics of the downward flux of
617 particles and carbon in the open northwestern Mediterranean Sea. Deep Sea Res. 41, 243-261.
618 Miquel J. C. and La Rosa J., 2001. Suivi à long terme des flux particulaires au site DYFAMED (Mer
619 Ligure, Méditerranée Occidentale). *Océanis* 25, 303-318.
620 Narita H., Abe R., Tate K., Kim Y., Harada K., and Tsunogai S., 2003. Anomalous large scavenging
621 of ^{230}Th and ^{231}Pa controlled by particle composition in the northwestern North Pacific. J.
622 Oceanogr. 59(739–750).
623 Pham M. K., La Rosa J. J., Lee S. H., Oregioni B., and Povinec P. P., ., 2005. Deposition of Saharan
624 dust in Monaco rain 2001-2002: Radionuclides and elemental composition. Physica Scripta 118,
625 14-17.

626 Quigley M. S., Santschi P. H., Hung C. C., Guo L. D., and Honeyman B. D., 2002. Importance of acid
627 polysaccharides for Th-234 complexation to marine organic matter. Limnol. Oceanogr. 47, 367-
628 377.
629 Ridame C., Guieu C., and Loye-Pilot M. D., 1999. Trend in total atmospheric deposition fluxes of
630 aluminium, iron and trace metals in the North western Mediterranean, over the past decade
631 (1985– 1997). J. Geophys. Res. 104, 127–138.
632 Roy-Barman M., Chen J. H., and Wasserburg G. J., 1996. ^{230}Th-^{232}Th systematics in the Central
633 Pacific Ocean: the sources and the fates of thorium. Earth Planet. Sci. Lett. 139, 351-363.
634 Roy-Barman M., Coppola L., and Souhaut M., 2002. Thorium isotopes in the Western Mediterranean
635 Sea: an insight into the marine particle dynamics. Earth Planet Sci. Lett. 196, 161-174.
636 Roy-Barman M., Jeandel C., Souhaut M., Rutgers van der Loeff M., Voege I., Leblond N., and
637 Freydier R., 2005. The influence of particle composition on thorium scavenging in the NE
638 Atlantic ocean (POMME experiment). Earth Planet. Sci. Lett. 240, 681– 693.
639 Sarthou G. and Jeandel C., 2001. Seasonal variations of iron concentrations in the Ligurian Sea and
640 iron budget in the Western Mediterranean Sea. Mar. Chem. 74, 115-129.
641 Schmidt S., Andersen V., Belviso S., and Marty J.-C., 2002. Strong seasonality in particle dynamics
642 of north-western Mediterranean surface waters as revealed by ^{234}Th/^{238}U. Deep Sea Res. 49,
643 1507-1518.
644 Schmidt S., Nival P., Reyss J.-L., Baker M., and Buat-Menard P., 1992. Relation between ^{234}Th
645 scavenging and zooplancton biomass in Mediterranean surface waters. Oceanol. Acta 15, 227-
646 231.

647 Scholten J. C., Fietzke J., Mangini A., Stoffers P., Rixen T., Gaye-Haake B., Blanze T., Ramaswamy
648 V., Sirocko F., Schulzh H., and Ittekkot V., 2005. Radionuclide fluxes in the Arabian Sea: the
649 role of particle composition. Earth Planet. Sci. Lett. 230, 319-337.
650 Scholten J. C., Fietzke_ J., Vogler S., Rutgers van der Loeff_ M. M., Mangini A., Koeve_ W.,
651 Waniek_ J., Sto!ers_ P., Antia_ A., and Kuss J., 2001. Trapping efficiencies of sediment traps
652 from the deep Eastern North Atlantic: the ^{230}Th calibration. Deep-Sea Res. II 48, 2383-2408.
653 Sempéré R., Yoro S. C., Van Wambeke F., and Charrière B., 2000. Microbial decomposition of large
654 organic particles in the northwestern Mediterranean Sea. An experimental approach. Mar. Ecol.
655 Prog. Ser. 198, 61-72.
656 Sicre M.-A., Ternois Y., Miquel J.-C., and Marty J.-C., 1999. Alkenone in the Northwestern
657 Mediterranean sea: interannual variability and vertical transfer. Geophys. Res. Lett. 26, 1735-
658 1738.
659 Siddall M., Henderson G. M., Edwards N. R., Müller S. A., Stocker T. F., Joos F., and Frank M.,
660 2005. ^{231}Pa/^{230}Th fractionation by ocean transport, biogenic particle flux and particle type. Earth
661 Planet. Sci. Lett. 237, 137–155.
662 Stemmann L., Gorsky G., Marty J.-C., Picheral M., and Miquel J.-C., 2002. Four-year study of large-
663 particle vertical distribution (0–1000 m) in the NW Mediterranean in relation to hydrology,
664 phytoplankton, and vertical flux. Deep-Sea Res. II 49, 2143–2162.
665 Sternberg E., Jeandel C., Miquel J.-C., Gasser B., Souhaut M., Arraes-Mescoff R., and Francois R.,
666 2007. Particulate barium fluxes and export production in the northwestern Mediterranean. Mar.
667 Chem. 105, 281–295.
668 Taylor S. R. and McLennan S. M., 1995. The Geochemical Evolution of the Continental Crust. Rev.
669 Geophys. 33, doi:10.1029/95RG00262.

Ternois Y., Sicre M.-A., Boireau A., Marty J.-C., and Miquel J.-C., 1996. Production pattern of alkenones in the Mediterranean sea. Geophys. Res. Lett. 23(3171-3174).

Trimble S. M., Baskarana M., and Porcelli D., 2004. Scavenging of thorium isotopes in the Canada Basin of the Arctic Ocean. Earth. Planet. Sci. Lett. 222, 915-932.

Usbeck R., Schlitzer R., Fischer G., and Wefer G., 2003. Particle fluxes in the ocean: comparison of sediment trap data with results from inverse modelling. J. Mar. Systems 39, 167-183.

Yu E.-F., Francois R., Bacon M. P., Honjo S., Fleer A. P., Manganini S. J., Rutgers van der Loeff M. M., and Ittekot V., 2001. Trapping effciency of bottom-tethered sediment traps estimated from the intercepted fluxes of ^{230}Th and ^{231}Pa. Deep-Sea Res. I 48, 865-889.

681

Table 1: sediment trap data

sample	Sampling dates	mass flux ($mg/m^2/d$)	^{232}Th (ppm)	^{230}Th (ppt)	$^{230}Th/^{232}Th$ (mol/mol)	U (ppm)	U_{lith} (ppm)	$^{230}Th_{xs}$ (ppt)	Al (w%)	Mn (ppm)	Mn_{auth} (ppm)	Ba (ppm)	Ba_{ex} (ppm)	POC (w%)	$CaCO_3$ (w%)
200 m															
1B	15.07.99-08.08.99	5.8	1.87 ± 0.01	11.6 ± 0.8	6.2 ± 0.4	0.49	0.24 ± 0.25	7.6 ± 5.0	1.18	157	58 ± 12	347	268 ± 20	14	47
2B	09.08.99-05.09.99	25.8	7.95 ± 0.05	46.3 ± 0.7	5.8 ± 0.1	1.76	1.66 ± 0.12	19.1 ± 2.6	5.58	787	315 ± 58	673	300 ± 76	13	14
3B	06.09.99-03.10.99	4.0	4.66 ± 0.02	24.7 ± 0.9	5.3 ± 0.2	1.10	0.80 ± 0.31	11.7 ± 6.0	3.45	287	-5 ± 32	454	223 ± 48	9	40
4B	04.10.99-31.10.99	16.5	5.61 ± 0.02	30 ± 1.4	5.4 ± 0.2	1.28	1.08 ± 0.22	12.6 ± 5.0	3.91	332	1 ± 36	617	356 ±56	11	27
5B	01.11.99-05.12.99	9.0	7.10 ± 0.02	33.2 ± 0.9	4.7 ± 0.1	1.38	1.18 ± 0.21	13.8 ± 4.4	4.66	512	117 ± 46	625	313 ± 65	16	27
6B	13.12.99-09.01.00	100	8.07 ± 0.03	34.2 ± 0.6	4.2 ± 0.1	1.65	1.55 ± 0.14	8.8 ± 3.0	5.92	852	351 ± 62	548	153 ± 77	11	13
7B	10.01.00-30.01.00	97	9.85 ± 0.07	39.7 ± 0.5	4.0 ± 0.1	1.86	1.75 ± 0.12	11.0 ± 2.5	6.99	850	258 ± 70	506	39 ± 89	14	15
8B	31.01.00-20.02.00	223	9.89 ± 0.07	40 ± 1.2	4.1 ± 0.1	2.05	1.98 ± 0.08	7.7 ± 2.5	6.89	872	288 ± 70	333	-127 ± 84	12	9
9B	21.02.00-12.03.00	222	9.34 ± 0.06	39.3 ± 0.5	4.2 ± 0.1	1.98	1.89 ± 0.12	8.4 ± 2.5	6.45	779	233 ± 65	462	31 ± 82	13	12
10B	13.03.00-26.03.00	315	6.38 ± 0.03	27.8 ± 0.6	4.4 ± 0.1	1.35	1.30 ± 0.09	6.5 ± 2.0	5.37	640	185 ± 54	399	40 ± 68	8	7
11B	03.04.00-09.04.00	813	0.90 ± 0.01	4.9 ± 0.3	5.4 ± 0.3	0.43	0.34 ± 0.10	-0.6 ± 1.8	0.93	48	-31 ± 8	321	259 ± 17	4	12
12B	10.04.00-01.05.00	434	2.13 ± 0.01	11.0 ± 0.3	5.2 ± 0.1	0.75	0.60 ± 0.16	1.2 ± 2.8	1.77	114	-36 ± 16	264	146 ± 25	14	20
13B	01.05.00-21.05.00	267	1.87 ± 0.01	10.2 ± 0.4	5.4 ± 0.2	0.65	0.49 ± 0.17	2.2 ± 3.2	1.79	172	20 ± 17	415	295 ± 28	18	22
14B	22.05.00-11.06.00	134	2.00 ± 0.01	11.6 ± 0.5	5.8 ± 0.2	0.64	0.50 ± 0.15	3.5 ± 2.9	1.62	259	121 ± 18	567	459 ± 30	17	19
15B	12.06.00-25.06.00	537	1.32 ± 0.01	8.0 ± 0.3	6.0 ± 0.3	0.47	0.37 ± 0.11	1.9 ± 2.2	0.92	133	55 ± 10	343	281 ± 17	31	14
16B	26.06.00-09.07.00	78	1.28 ± 0.01	8.2 ± 0.3	6.4 ± 0.3	0.41	0.30 ± 0.12	3.4 ± 2.3	0.76	124	60 ± 8	276	225 ± 14	29	16
17B	10.07.00-16.07.00	536	1.80 ± 0.01	10.7 ± 0.4	6.0 ± 0.2	0.65	0.53 ± 0.12	2.0 ± 2.4	1.23	127	23 ± 12	377	295 ± 21	29	15
1000 m															
1A	15.07.99-08.08.99	68	6.80 ± 0.13	45 ± 1.2	6.7 ± 0.2	1.55	1.47 ± 0.09	21.3 ± 2.6	5.00	871	448 ± 55	823	489 ± 73	12	11
2A	09.08.99-05.09.99	123	8.10 ± 0.13	45 ± 2.6	5.6 ± 0.3	1.73	1.63 ± 0.11	18.7 ± 4.3	5.65	716	237 ± 57	674	296 ± 77	12	13
3A	06.09.99-03.10.99	61	6.76 ± 0.06	40.3 ± 0.7	6.0 ± 0.1	1.59	1.51 ± 0.09	15.5 ± 2.1	4.95	638	220 ± 50	643	313 ± 68	12	10
4A	04.10.99-31.10.99	42	7.51 ± 0.04	47 ± 0.6	6.3 ± 0.1	1.79	1.69 ± 0.11	19.3 ± 2.3	5.09	671	240 ± 52	797	457 ± 73	13	12
5A	01.11.99-05.12.99	9.8	6.82 ± 0.04	42 ± 1.0	6.2 ± 0.2	1.59	1.50 ± 0.10	17.7 ± 2.6	4.67	610	215 ± 48	679	367 ± 66	10	11
6A	13.12.99-09.01.00	8.3	4.89 ± 0.02	27 ± 1.1	5.5 ± 0.2	1.08	0.96 ± 0.14	11.0 ± 3.4	3.52	449	151 ± 36	471	236 ± 49	17	16
7A	10.01.00-30.01.00	20	9.21 ± 0.03	41 ± 1	4.4 ± 0.1	1.78	1.71 ± 0.08	12.7 ± 2.3	6.45	821	275 ± 66	575	144 ± 84	10	9
8A	31.01.00-20.02.00	165	4.80 ± 0.01	32.4 ± 0.5	6.8 ± 0.1	1.40	1.36 ± 0.05	10.3 ± 1.4	3.91	509	179 ± 40	784	523 ± 60	9	5
9A	21.02.00-12.03.00	129	9.39 ± 0.10	43.9 ± 0.7	4.7 ± 0.1	2.06	2.02 ± 0.06	10.9 ± 1.7	6.61	857	297 ± 68	502	60 ± 84	8	6
10A	13.03.00-26.03.00	283	8.81 ± 0.06	42.4 ± 0.7	4.8 ± 0.1	1.90	1.86 ± 0.06	12.1 ± 1.8	6.02	801	291 ± 62	479	76 ± 77	9	6
11A	03.04.00-09.04.00	298	2.74 ± 0.02	17.5 ± 0.5	6.4 ± 0.2	1.00	0.90 ± 0.12	2.8 ± 2.5	2.24	244	54 ± 22	491	341 ± 35	5	13
12A	10.04.00-01.05.00	311	3.55 ± 0.03	22.9 ± 0.4	6.4 ± 0.1	1.18	1.10 ± 0.08	4.8 ± 1.8	3.04	333	76 ± 30	507	304 ± 44	9	10
13A	01.05.00-21.05.00	227	9.32 ± 0.03	42.1 ± 0.5	4.5 ± 0.1	1.96	1.88 ± 0.10	11.2 ± 2.2	6.76	921	349 ± 70	438	-14 ± 85	12	10
14A	22.05.00-11.06.00	289	3.06 ± 0.01	22.5 ± 0.4	7.4 ± 0.1	0.80	0.70 ± 0.11	11.1 ± 2.2	2.60	304	84 ± 26	587	413 ± 41	16	13
15A	12.06.00-25.06.00	528	2.81 ± 0.03	19.5 ± 0.5	6.9 ± 0.2	0.85	0.77 ± 0.09	6.9 ± 2.0	2.11	355	176 ± 23	576	435 ± 35	25	11
16A	26.06.00-09.07.00	277	2.79 ± 0.01	19.3 ± 0.4	6.9 ± 0.2	0.70	0.60 ± 0.10	9.4 ± 2.0	2.07	389	213 ± 24	721	582 ± 38	27	12
17A	10.07.00-16.07.00	422	4.30 ± 0.02	28.8 ± 0.6	6.7 ± 0.1	1.07	0.95 ± 0.13	13.2 ± 2.8	3.27	450	174 ± 34	846	628 ± 54	21	16

Table 2: Partition coefficient of Th between lithogenic particles, MnO_2 and seawater

	$K_{d\text{-}litho}^{Th}$ (10^7 ml/g)	$K_{d\text{-}MnO2}^{Th}$ (10^{10} ml/g)
DYFAMED 1000 m, main correlation (this work)	0.8 ± 0.2	1.1 ± 0.4
DYFAMED 1000 m, winter samples (this work)	0.42 ± 0.04	0.6 ± 0.1
Eastern North Atlantic[1]	5	2
Eastern North Atlantic[2]	0.5-10	0.7-4.2
North Atlantic[3]	1	
Equatorial Pacific and Southern Ocean[4]	23	
Equatorial Pacific and Southern Ocean [5]	20	3.5
Panama Basin[6]	2-4	0.6-3.7

[1] Roy-Barman et al., 2005. [2] Scholten et al., 2001; Kuss and Kremling, 1999. [3] Chase et al., 2002. [4] Luo and Ku, 2004a; Luo and Ku, 2004b. [5] Luo and Ku, 1999, (unpublished data, 1993, http://usjgofs.whoi.edu/jg/dir/jgofs/eqpac/tt013/. [6] Anderson et al., 1983 (restricted to the samples with a sufficient Mn_{auth} content).

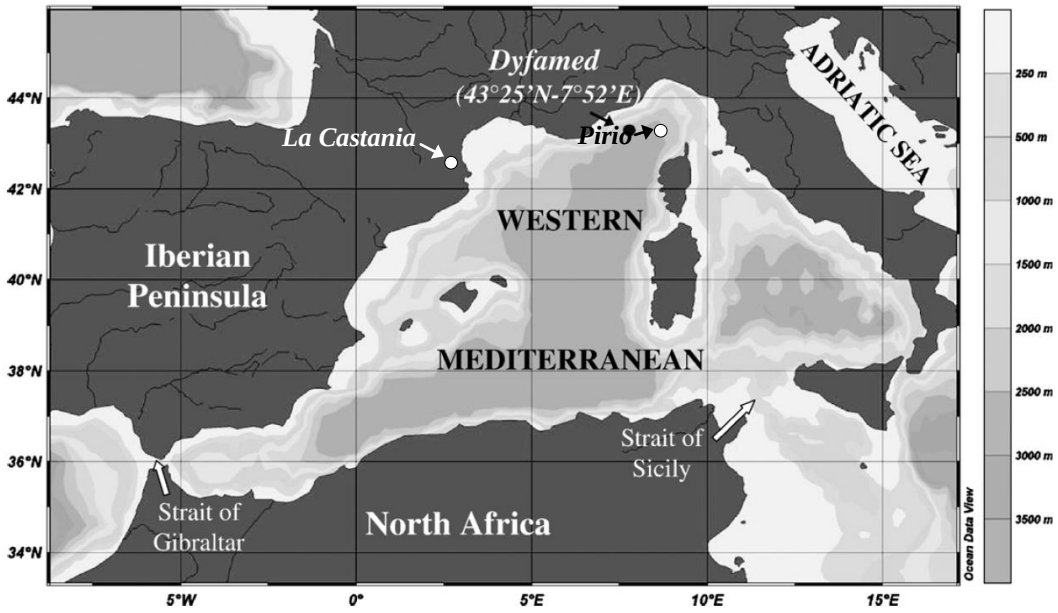
Dyfamed
(43°25'N-7°52'E)
La Castania
Piriò
ADRIATIC SEA
WESTERN
MEDITERRANEAN
Iberian
Peninsula
North Africa
Strait of
Sicily
Strait of
Gibraltar
44°N
42°N
40°N
38°N
36°N
34°N
5°W
0°
5°E
10°E
15°E
250 m
500 m
1000 m
1500 m
2000 m
2500 m
3000 m
3500 m
Ocean Data View

Figure 1

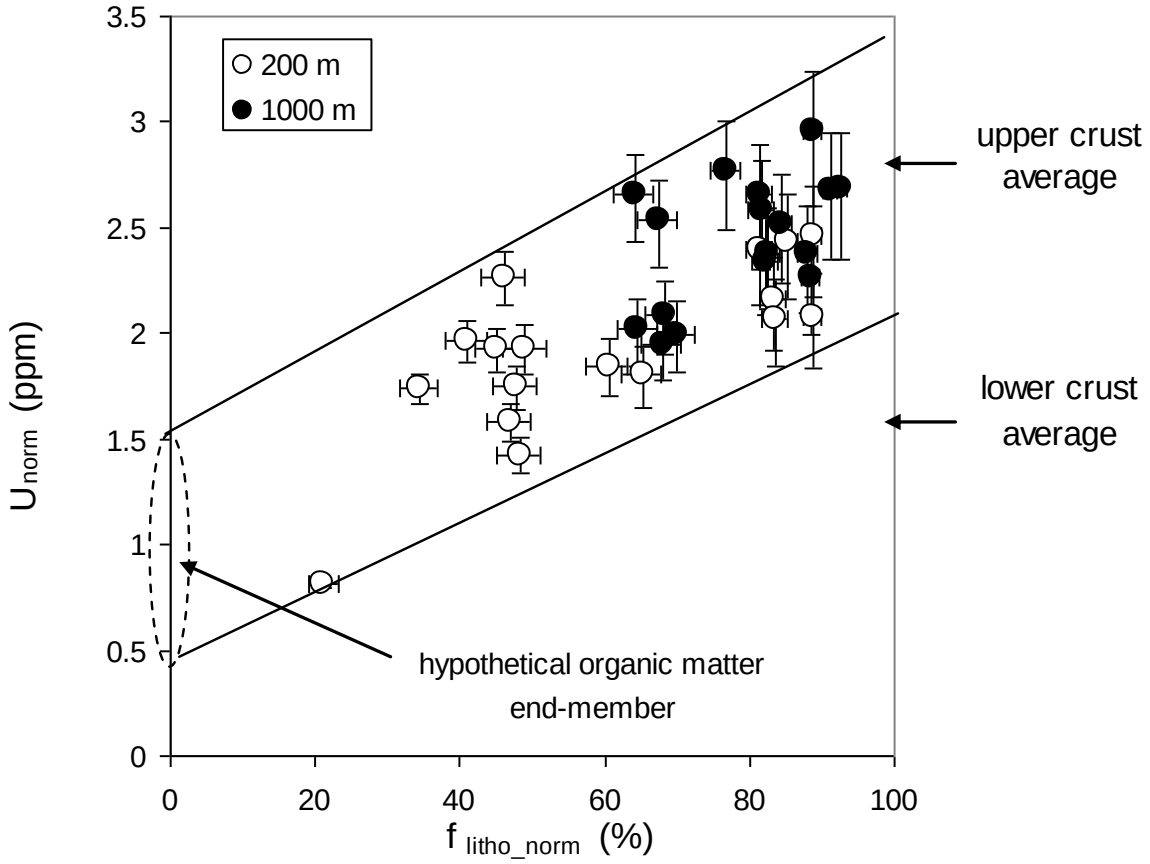
200 m
1000 m
upper crust
average
lower crust
average
hypothetical organic matter
end-member
U norm (ppm)
f litho_norm (%)
0
0.5
1
1.5
2
2.5
3
3.5
0
20
40
60
80
100

Figure 2

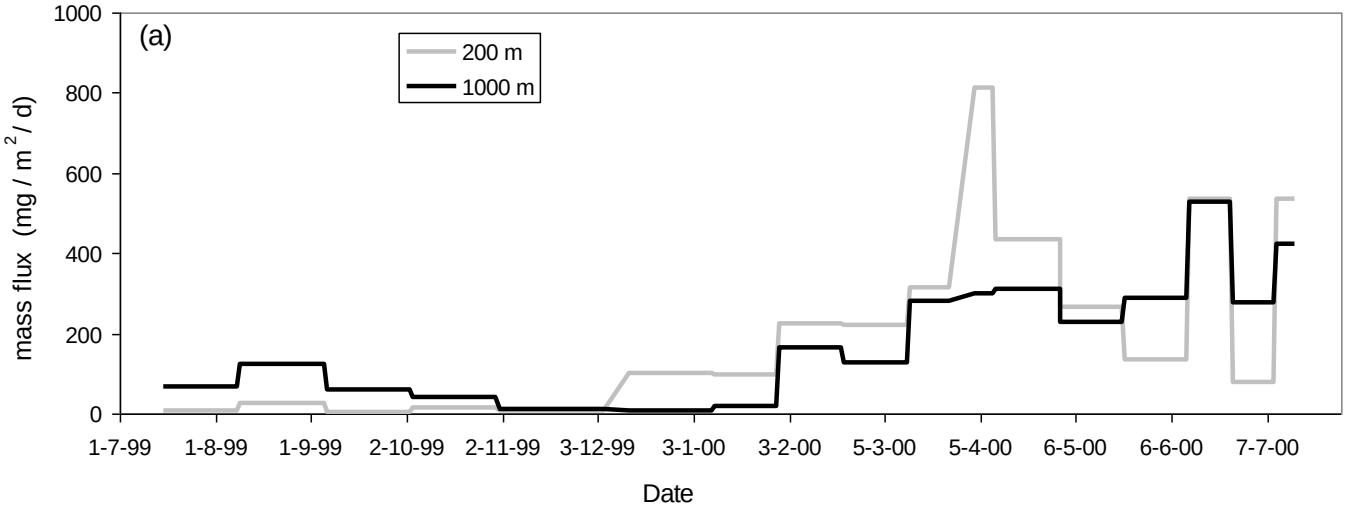
(a)
200 m
1000 m
mass flux (mg / m 2 / d)
1000
800
600
400
200
0
1-7-99
1-8-99
1-9-99
2-10-99
2-11-99
3-12-99
3-1-00
3-2-00
5-3-00
5-4-00
6-5-00
6-6-00
7-7-00
Date

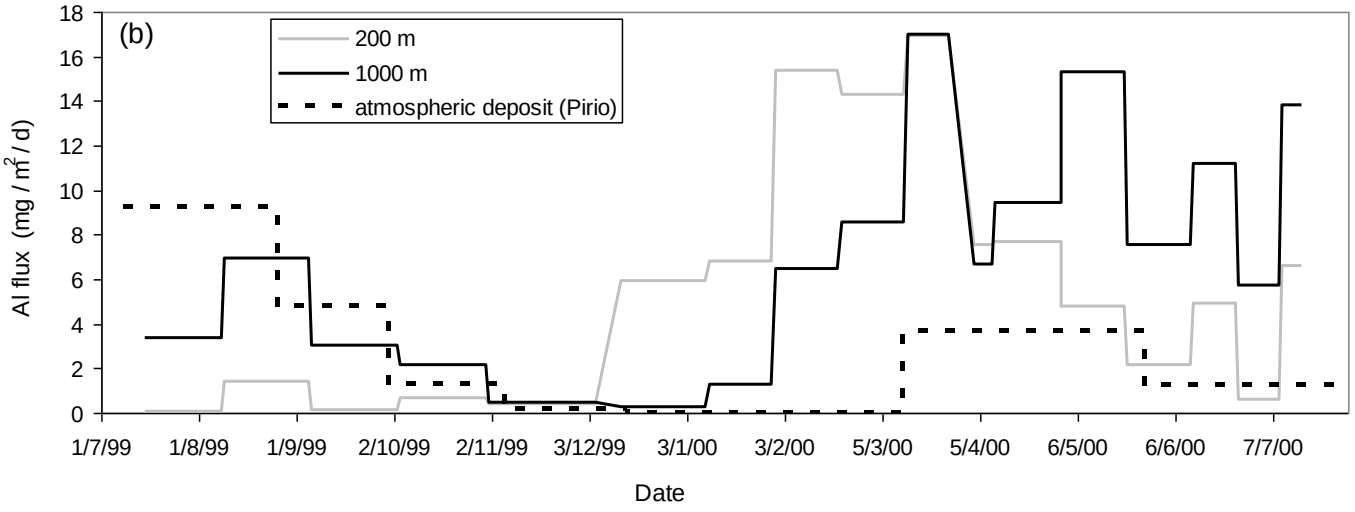
(b)
200 m
1000 m
atmospheric deposit (Pirio)
Al flux (mg / m2 / d)
18
16
14
12
10
8
6
4
2
0
1/7/99
1/8/99
1/9/99
2/10/99
2/11/99
3/12/99
3/1/00
3/2/00
5/3/00
5/4/00
6/5/00
6/6/00
7/7/00
Date

Figure 3

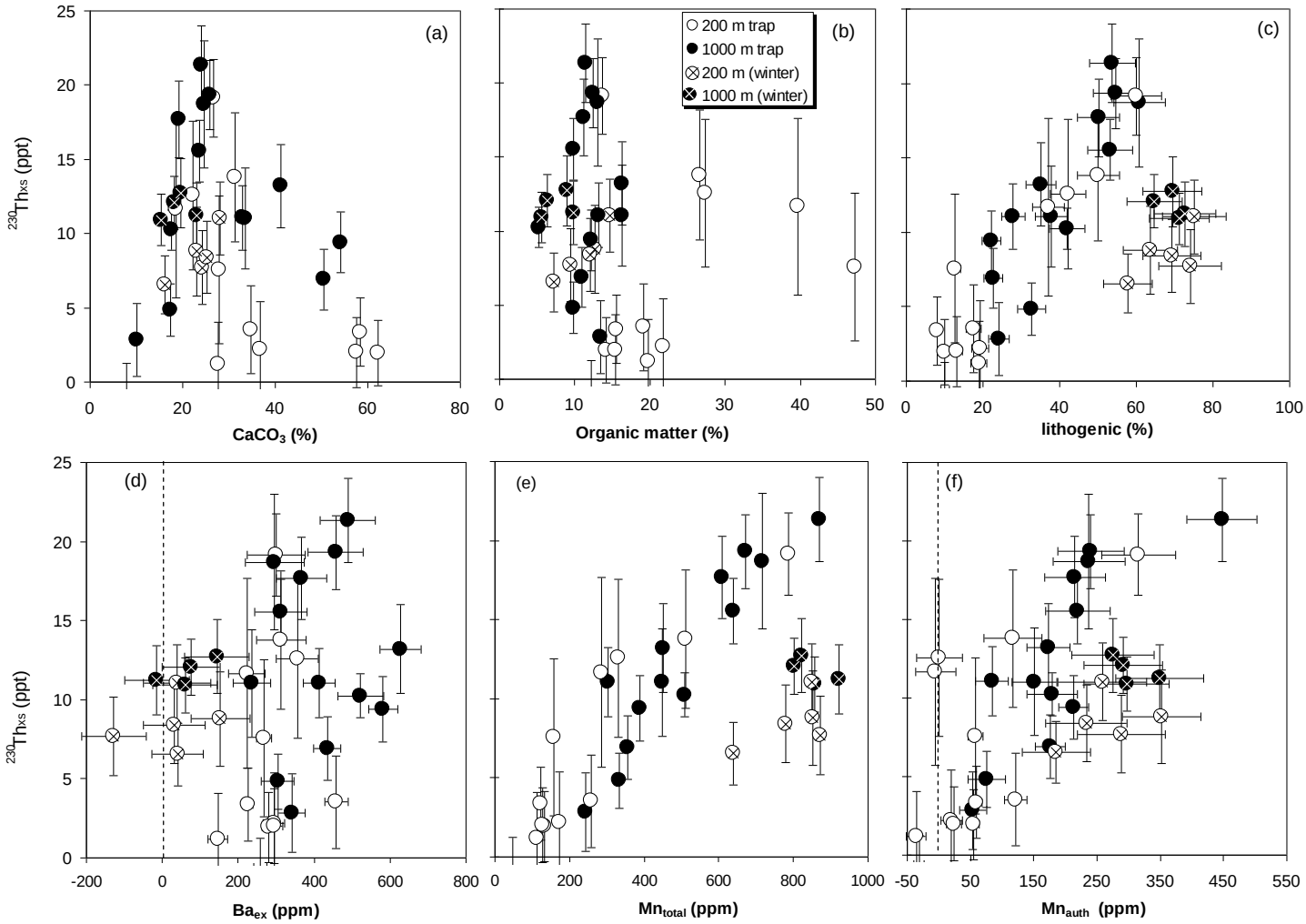
(a)
(b)
(c)
(d)
(e)
(f)
200 m trap
1000 m trap
200 m (winter)
1000 m (winter)
$^{230}Th_{xs}$ (ppt)
$CaCO_3$ (%)
Organic matter (%)
lithogenic (%)
Ba_{ex} (ppm)
Mn_{total} (ppm)
Mn_{auth} (ppm)

Figure 4